RSC Advances

PAPER

View Article Online
View Journal | View Issue

Cite this: *RSC Adv.*, 2019, **9**, 2740

Theoretical prediction of HfB_2 monolayer, a two-dimensional Dirac cone material with remarkable Fermi velocity†

Zhongfei Liu,[a] Peihong Wang,[a] Qiaoyu Cui,[a] Guang Yang,[b] Shaowei Jin *[ac] and Kuangwei Xiong*[d]

Received 7th October 2018
Accepted 26th December 2018

DOI: 10.1039/c8ra08291j

rsc.li/rsc-advances

Searching for new two-dimensional (2D) Dirac cone materials has been popular since the discovery of graphene with a Dirac cone structure. Based on density functional theory (DFT) calculations, we theoretically designed a HfB_2 monolayer as a new 2D Dirac material by introducing the transition metal Hf into a graphene-like boron framework. This newly predicted HfB_2 monolayer has pronounced thermal and kinetic stabilities along with a Dirac cone with a massless Dirac fermion and Fermi velocities (3.59×10^5 and 6.15×10^5 m s^{-1}) comparable to that of graphene (8.2×10^5 m s^{-1}). This study enriches the diversity and promotes the application of 2D Dirac cone materials.

Introduction

Since the discovery of graphene by Novoselov *et al.*,[1] two-dimensional (2D) materials with Dirac cones, which are characterized by linear dispersion bands in the vicinity of the Fermi level, have garnered tremendous interest due to their unconventional properties, such as half-integer,[2,3] fractional[4–6] and fractal[7] quantum Hall effects along with ultra-high carrier mobility.[8,9] These fascinating characteristics have promoted the exploration of other 2D Dirac cone materials. Given the rigorous requirements for the existence of Dirac cones in 2D materials, to date, only graphene,[2] silicone and germanene,[10] carbon allotropes,[11–13] boron allotropes[14–16] and a handful of other systems[17–21] have been verified to be Dirac cone materials.

Boron atom exhibits flexible bonding characteristics because its three valence electrons can occupy four available orbitals. Attempting to compensate for the electron deficiency boron is an effective strategy to form an isoelectronic structure like carbon. Based on this strategy, some 2D boron-based Dirac materials including monolayer TiB_2,[22] single-layer FeB_2,[23] and hydrogenated boron sheets have been predicted.[24] In these boron-based Dirac materials, freestanding monolayer TiB_2 sheets tend to bend into tubular shapes and exhibit bending instability; thus, planar TiB_2 needs to be stabilized on a substrate. In addition, other 2D boron-based materials in the *P6/mmm* space group, such as MgB_6 (ref. 25) and MnB_6 (ref. 26), are not Dirac materials, although they have stable structures. Therefore, exploring boron-based compounds for new 2D Dirac cone materials is a priority in both experimental and theoretical efforts.

In this paper, we theoretically predict a new 2D Dirac material, HfB_2 monolayer, with Fermi velocities of 3.59×10^5 and 6.15×10^5 m s^{-1}. We embedded the electron-rich transition metal Hf ($5d^26s^2$) into a graphene-like boron network to stabilize the unstable boron sheets. The band structures of HfB_2 display a Dirac cone at the high-symmetric K point in the absence of spin–orbit coupling (SOC). Meanwhile, the predicted HfB_2 monolayer presents ultra-high maximum Fermi velocities of 3.59×10^5 and 6.15×10^5 m s^{-1} along with excellent thermodynamic stability. Our analysis of monolayer HfB_2 provides theoretical guidance for predicting and developing 2D Dirac materials.

Computational method

For first-principles calculations, the Vienna *Ab initio* Simulation Package (VASP)[27] was employed within the framework of the Perdew–Burke–Ernzerhof (PBE)[28] generalized gradient approximation. Ion–electron interactions were treated by the projector augmented wave method.[29] The energy cutoff was set to 600 eV, and the energy precision was set to 10^{-5} eV. Geometries were fully relaxed until the residual force on each atom was less than 10^{-4} eV Å^{-1}. In the geometry optimization and self-consistent computations, the first Brillouin zone was sampled with a $9 \times 9 \times 1$ Γ-centered Monkhorst–Pack *k*-point grid. The Heyd–

[a]*School of Physics and Materials Science, Anhui University, Hefei 230601, P. R. China. E-mail: jinsw@mail.ustc.edu.cn*

[b]*College of Energy and Environmental Engineering, Hebei University of Engineering, Handan 056038, Hebei Province, P. R. China*

[c]*Anhui Key Laboratory of Information Materials and Devices, Hefei 230601, Anhui Province, P. R. China*

[d]*Department of Physics, East China Jiaotong University, Nanchang 330013, Jiangxi Province, P. R. China*

† Electronic supplementary information (ESI) available. See DOI: 10.1039/c8ra08291j

Scuseria–Ernzerhof (HSE06)[30] hybrid functional was used to calculate more reliable band structures.

A vacuum layer larger than 15 Å was used to avoid interactions between neighboring layers. The dynamic stabilities of HfB_2 were checked based on the phonon dispersion spectra, as implemented in the phonopy code,[31] interfaced with density functional perturbation theory implemented in VASP. Thermal stability was evaluated *via ab initio* molecular dynamics (AIMD) simulations in the NVT ensemble at temperatures of 300, 500, 800 and 1200 K. The temperature was controlled using the Nosé–Hoover method.[32] The computational benchmarks are detailed in the ESI (Fig. S1).†

Results and discussion

Graphene-like boron sheets are unstable since there are only six electrons for each boron atom. Thus, additional atoms are needed to complete the outer electron shell. Embedding the electron-rich metal Hf into graphene-like boron layers can stabilize the boron sheets. The top view and side view of the optimized structure of monolayer HfB_2 is shown in Fig. 1. As seen in Fig. 1, the 2D HfB_2 monolayer belongs to the space group *P*6/*mmm*, in which B atoms are arranged in a honeycomb structure, and each Hf atom coordinates with six members of boron rings to form a quasi-planar hexacoordination. The quasi-planar structure of the HfB_2 monolayer is as a result of spontaneous symmetry lowering due to Pseudo Jahn–Teller instability in its planar form.[33–37]

The B–B and B–Hf bond lengths are 1.85 and 2.32 Å, respectively. The vertical distance between the Hf atom and B layer is 1.41 Å. The B–B bond length (1.85 Å) is almost equivalent to that in the FeB_2 monolayer (1.83 Å)[23] and slightly longer than those in the TiB_2 monolayer (1.79 Å),[22] hydrogenated boron sheet (1.72 Å)[24] and boron sheet (1.67 Å).[38] The B–Hf bond length (2.32 Å) is smaller than that in bulk HfB_2 (2.53 Å),[39] indicating a much stronger interaction between the Hf atoms and boron layer.

To assess the stability of the HfB_2 monolayer, we calculated its cohesive energy E_{coh}, which was defined as

$$E_{coh} = (nE_{Hf} + 2nE_B - nE_{HfB_2})/N, \quad (1)$$

where E_{Hf} and E_B are the total energies of a single Hf atom and B atom, respectively, E_{HfB_2} is the total energy of one unit cell of the HfB_2 monolayer, and N is the number of atoms in the supercell. The cohesive energy of the investigated HfB_2 monolayer is 6.12 eV per atom, which is comparable to those of the FeB_2 monolayer (4.87 eV per atom),[23] FeB_6 monolayer (5.56–5.79 eV per atom),[40] and B_2S monolayer (5.3 eV per atom).[17] The comparable cohesive energies of HfB_2 monolayer (6.12 eV per atom) and FeB_6 monolayer (5.56–5.79 eV per atom) suggest that the HfB_2 monolayer has the same type of chemical bonds as the FeB_6 monolayer. The large cohesive energy also indicates that the HfB_2 sheet is energetically favorable.

We also computed the phonon spectrum to check the kinetic stabilities of the HfB_2 monolayer (Fig. 2). A tiny imaginary frequency was found near the Γ point. This phenomenon was also found in the phonon spectra of germanene,[10] borophene,[41] arsenene[42] and other two-dimensional systems.[43] It is not a sign of structural instability and may be the result of numerical instability when accurately calculating rapidly decreasing interatomic forces.[43] Our analysis of the phonon dispersion curves suggests that the HfB_2 sheet can be dynamically stable.

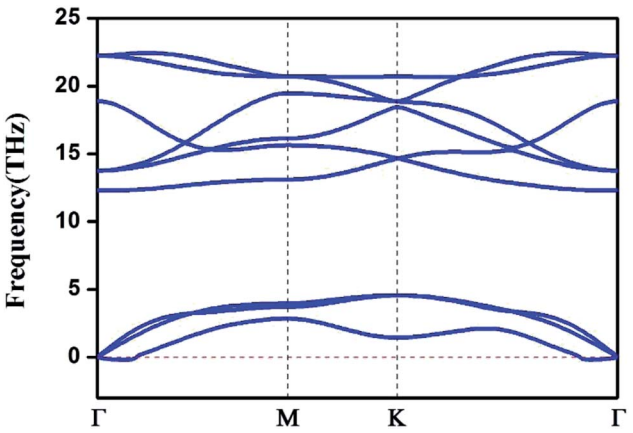

Fig. 2 Phonon dispersion spectrum of the HfB_2 monolayer.

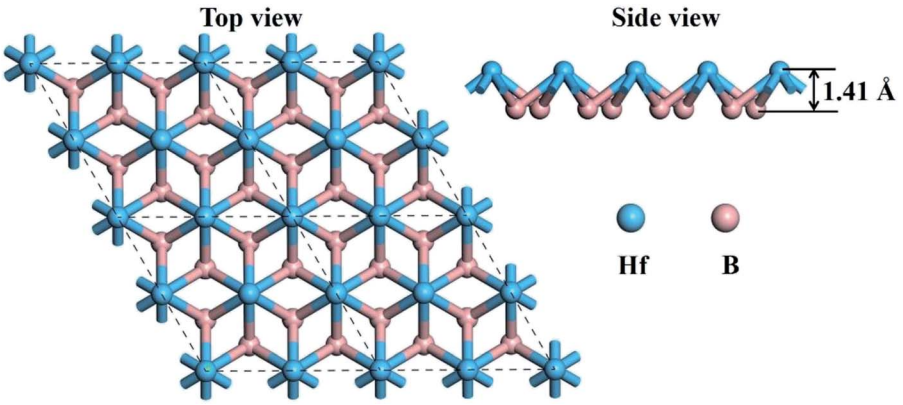

Fig. 1 Top view and side view of the optimized geometry of the HfB_2 monolayer.

We then carried out AIMD simulations to examine the thermal stability of HfB_2 monolayer at the temperatures of 300, 400, 500, and 800 K. A $5 \times 5 \times 1$ supercell was adopted to reduce the constraints of the periodic boundary conditions. As shown in Fig. 3, the HfB_2 monolayer does not undergo obvious structural distortion at 400 K. However, drastic structure collapse is observed at 500 K. In particular, the hexacoordination of Hf atom transfers to an even higher coordination at the temperatures of 500 and 800 K. The above results suggest that the HfB_2 monolayer is stable at room temperature.

According to the calculated cohesive energies, phonon spectra and AIMD simulations, the predicted HfB_2 monolayer have pronounced thermodynamic stability. Therefore, we next investigated its band structure and corresponding projected density of states (PDOS). As shown in Fig. 4a, two bands cross each other linearly around the Fermi level, which creates an intrinsic Dirac cone. The meeting point of the conduction band (CB) and valence band (VB) is located at the high-symmetry K (1/3, 1/3, 0) point. The PDOS shows that the VB and CB near the Fermi level mainly originate from hybridized Hf-s, Hf-d and B-p orbitals.

To confirm the existence of the Dirac cone, we recalculated the band structure using the HSE06 hybrid functional, which has been shown to be more reliable in the calculation of electronic structures.[44–48] Fig. 4b shows that the Dirac cone still exists (Fig. 4c and d show the enlarged band structure approach to the Dirac cone). The three-dimensional (3D) plot (Fig. 4e) exhibits a notable conical feature near the Fermi level. It is believed that the Dirac cone is a lower energy configuration compared to the Fermi level in the HfB_2 monolayer, which is a property intrinsic to this system.

Considering the strong SOC effect of Hf atoms, which might open up the band gap, we further investigated the effect of SOC on the electronic structure using the HSE06 hybrid functional method. The SOC effect introduces a gap of 146 meV (Fig. S2, ESI†), which is mainly due to the orbital contribution close to the nucleus. Additionally, the band lines crossing the Fermi level suggest the metallic property of the HfB_2 monolayer in consideration of the SOC effect.

The linear dispersion of the energy bands means that the carriers in CB and VB behave as Dirac fermions with zero mass, which results in excellent carrier transport characteristics near the Fermi level. We calculated the Fermi velocity ν_f of the HfB_2 monolayer with the expression $\nu_f = \partial E/(\hbar \partial k)$. The calculated maximum velocities were determined to be 3.59×10^5 m s^{-1} along the M $\rightarrow$ K direction and 6.15×10^5 m s^{-1} along the K $\rightarrow$ Γ direction using the HSE06 method. The velocities are comparable to those of graphene (8.2×10^5 m s^{-1})[49] and 2D boron-based Dirac cone materials such as FeB_2 monolayer (6.54×10^5 m s^{-1})[23] and B_2S monolayer (6.7×10^5 m s^{-1} along the k_x direction and 4.8×10^5 m s^{-1} along the k_y direction).[17]

Additionally, the Fermi velocity is largely arbitrary and strongly dependent on the stoichiometry along with the long-range geometry. To verify the reproducibility of these notable Fermi velocities, we also simulated the HfB_2 monolayer with one Hf atom replaced by a Zr atom ($Zr@HfB_2$). The dopant is

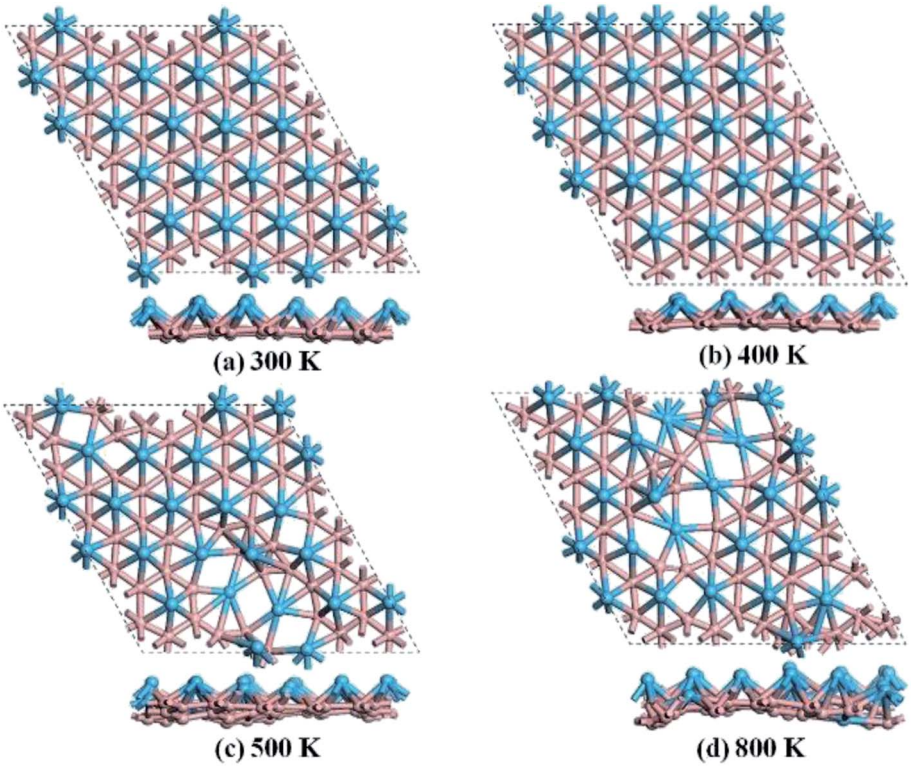

Fig. 3 Snapshots of the equilibrium structures of the HfB_2 monolayer after the *ab initio* molecular dynamics simulations at (a) 300 K, (b) 400 K, (c) 500 K, and (d) 800 K.

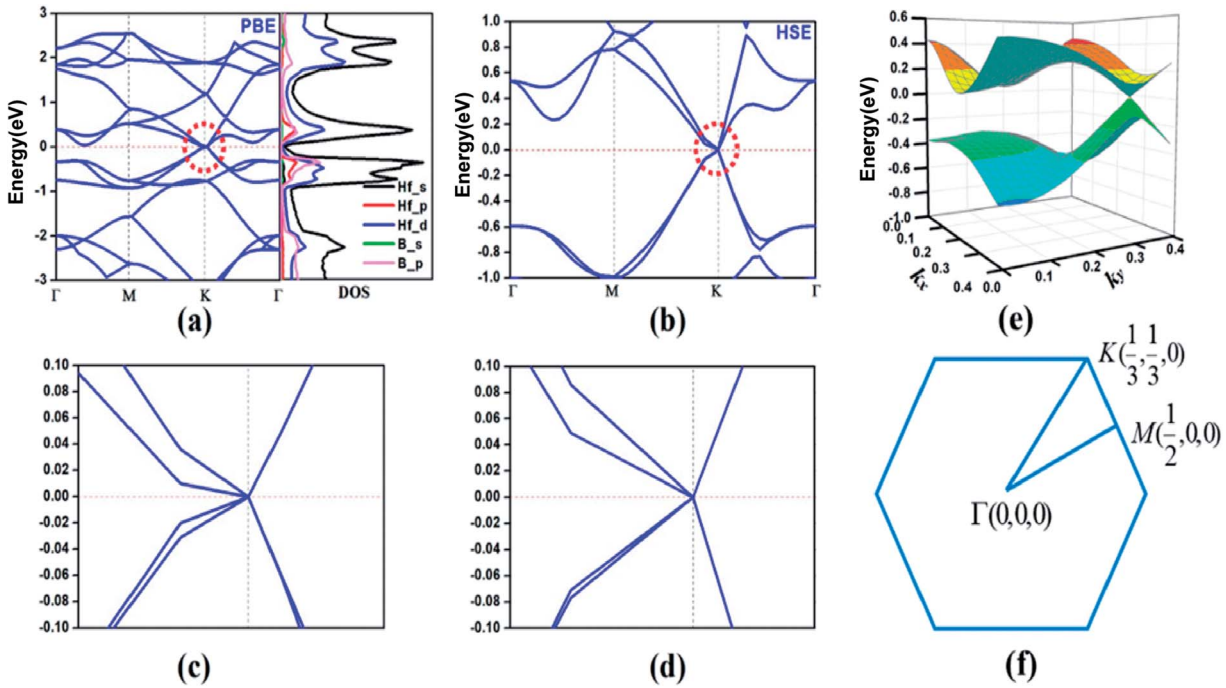

Fig. 4 (a) Band structures and projected density of states of the HfB_2 monolayer obtained using the PBE functional. The Fermi level is at 0 eV (red dashed lines). (b) Recalculated band structure obtained using the HSE06 hybrid functional. (c and d) Partial enlargement of the Dirac cone in (a and b). (e) Three-dimensional VB and CB along with the Dirac cone in the vicinity of the Fermi Level. (f) First Brillouin zone with the high-symmetry *k* points.

expected to induce distortions. Considering the high cost of HSE06 computations, the Fermi velocities of pure HfB_2 and $Zr@HfB_2$ monolayers were obtained by analyzing the band structure computed by PBE functionals (Fig. S3†). The PBE computations suggest that the Fermi velocities of $Zr@HfB_2$ are 4.40×10^3 m s^{-1} along the M → K direction and 9.10×10^3 m s^{-1} in the K → Γ direction, which are comparable to those of HfB_2 monolayer (5.46×10^3 and 7.74×10^3 m s^{-1},

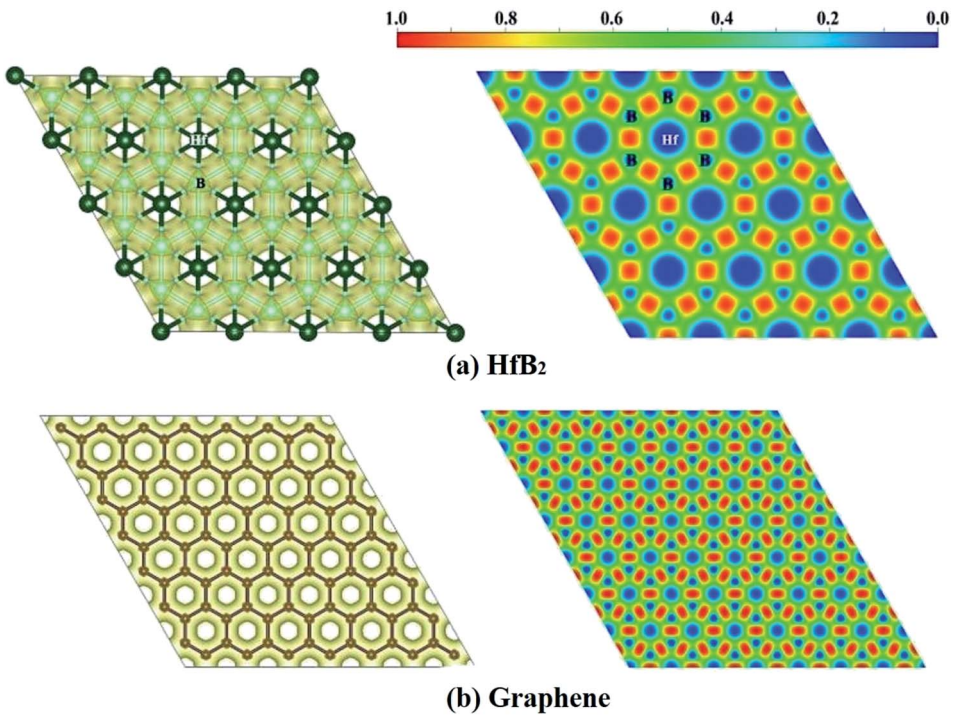

Fig. 5 ELF isosurfaces (left) plotted at the value of 0.50 au and ELF maps (right) for (a) HfB_2 monolayer and (b) graphene. Red and blue represent the highest (1.0) and lowest value (0.0) of ELF, respectively.

respectively). The above-mentioned Fermi velocities based on the PBE functionals are smaller than those obtained by the HSE06 method, which is due to the underestimation of the slopes of the band lines by the PBE method. Notably, the well-maintained Fermi velocities in Zr@HfB_2 with lattice distortion suggest that the remarkable Fermi velocities of HfB_2 monolayer are reproducible.

The strong connection between the Hf and B atoms suggest the experimental feasibility and thermodynamic stability of HfB_2 (Table S1†), which were confirmed by the phonon dispersion and AIMD results. We also computed the band structures of HgB_2, RuB_2, AuB_2 and IB_2 and found no Dirac cones within the band structures of these materials, with the exception of RuB_2 (Fig. S4†). The follow-up computations will be performed to further investigated the electronic properties of RuB_2. In addition, the HfB_2 monolayers with Hf atoms substituted by Ti and Zr atoms in the same main group were simulated, and no Dirac cones were found (Fig. S5†), indicating the unique characteristics of the HfB_2 sheet.

Finally, we computed the electron localization function (ELF)[50] of the HfB_2 monolayer to analyze its electron distribution. As shown in the ELF map in Fig. 5a, the electrons are mainly distributed around the B atoms, and remarkable electron transfer from Hf to B atoms is observed. The ELF map of HfB_2 monolayer is similar to that of graphene (Fig. 5b), which may be the root cause of the existence of the Dirac point.

From the perspective of the practical application of the predicted 2D HfB_2 monolayer, the HfB_2 film must be deposited on a suitable substrate.[51–53] We chose MoS_2 (lattice constant of 2 × 2 supercell: 6.30 Å) as a substrate to support the HfB_2 film (lattice constant of unit cell: 6.41 Å) to form the HfB_2@MoS_2 heterostructure, in which the lattice mismatch is only 1.7% (Fig. S6†). After full structural relaxation, the interlayer distance is 2.92 Å, and the binding energy is 45 meV per atom, which is comparable to that of the FeB_2/MoS_2 heterostructure and suggests the presence of van der Waals interactions between HfB_2 and the MoS_2 substrate.[23] From the above discussion, MoS_2 is an ideal substrate for the predicted HfB_2 monolayer to achieve potential device applications.

Based on the analysis of cohesive energies, phonon spectra, AIMD simulations and growth substrate, the HfB_2 monolayer is a 2D Dirac cone material with pronounced thermodynamic stability and experimental feasibility. In addition, the high carrier mobility and excellent electronic transport properties will likely make it a useful material in many fields, such as nanoelectronics, sensing and energy devices.

Conclusions

In summary, we successfully predicted a HfB_2 monolayer, a novel 2D boron-based Dirac cone material that can be constructed by embedding the electron-rich transition metal Hf into a graphene-like boron network. The HfB_2 monolayer is thermally and kinetically stable and possesses a promising Fermi velocity on the same order of magnitude as that of graphene. Orbital analysis shows that the Dirac cone near the Fermi level predominantly originates from hybridized Hf-s, Hf-d and B-p orbitals. Our work is expected to promote experimental efforts to synthesize predicted 2D boron-based Dirac materials and extend their applications in electronics.

Conflicts of interest

There are no conflicts to declare.

Acknowledgements

This work was supported by the Natural Science Foundation of China (61671017) and the Key Natural Science Research Program of Anhui Educational Committee (KJ2018ZD001, KJ2013A030).

Notes and references

1 K. S. Novoselov, A. K. Geim, S. V. Morozov, D. Jiang, Y. Zhang, S. V. Dubonos, I. V. Grigorieva and A. A. Firsov, *Science*, 2004, **306**, 666–669.
2 K. S. Novoselov, A. K. Geim, S. V. Morozov, D. Jiang, M. I. Katsnelson, I. V. Grigorieva, S. V. Dubonos and A. A. Firsov, *Nature*, 2005, **438**, 197–200.
3 Y. B. Zhang, Y. W. Tan, H. L. Stormer and P. Kim, *Nature*, 2005, **438**, 201–204.
4 K. I. Bolotin, F. Ghahari, M. D. Shulman, H. L. Stormer and P. Kim, *Nature*, 2009, **462**, 196–199.
5 X. Du, I. Skachko, F. Duerr, A. Luican and E. Y. Andrei, *Nature*, 2009, **462**, 192–195.
6 B. Hunt, J. D. Sanchez-Yamagishi, A. F. Young, M. Yankowitz, B. J. LeRoy, K. Watanabe, T. Taniguchi, P. Moon, M. Koshino, P. Jarillo-Herrero and R. C. Ashoori, *Science*, 2013, **340**, 1427–1430.
7 C. R. Dean, L. Wang, P. Maher, C. Forsythe, F. Ghahari, Y. Gao, J. Katoch, M. Ishigami, P. Moon, M. Koshino, T. Taniguchi, K. Watanabe, K. L. Shepard, J. Hone and P. Kim, *Nature*, 2013, **497**, 598–602.
8 K. I. Bolotin, K. J. Sikes, Z. Jiang, M. Klima, G. Fudenberg, J. Hone, P. Kim and H. L. Stormer, *Solid State Commun.*, 2008, **146**, 351–355.
9 E. H. Hwang and S. Das Sarma, *Phys. Rev. B: Condens. Matter Mater. Phys.*, 2008, **77**, 115449.
10 S. Cahangirov, M. Topsakal, E. Akturk, H. Sahin and S. Ciraci, *Phys. Rev. Lett.*, 2009, **102**, 236804.
11 Z. Wang, X. F. Zhou, X. Zhang, Q. Zhu, H. Dong, M. Zhao and A. R. Oganov, *Nano Lett.*, 2015, **15**, 6182–6186.
12 L. C. Xu, R. Z. Wang, M. S. Miao, X. L. Wei, Y. P. Chen, H. Yan, W. M. Lau, L. M. Liu and Y. M. Ma, *Nanoscale*, 2014, **6**, 1113–1118.
13 M. Zhao, W. Dong and A. Wang, *Sci. Rep.*, 2013, **3**, 3532.
14 H. Zhang, Y. Xie, Z. Zhang, C. Zhong, Y. Li, Z. Chen and Y. Chen, *J. Phys. Chem. Lett.*, 2017, **8**, 1707–1713.
15 X. F. Zhou, X. Dong, A. R. Oganov, Q. Zhu, Y. Tian and H. T. Wang, *Phys. Rev. Lett.*, 2014, **112**, 085502.
16 F. Ma, Y. Jiao, G. Gao, Y. Gu, A. Bilic, Z. Chen and A. Du, *Nano Lett.*, 2016, **16**, 3022–3028.

17 Y. Zhao, X. Li, J. Liu, C. Zhang and Q. Wang, *J. Phys. Chem. Lett.*, 2018, 1815–1820.
18 H. Pan, H. Zhang, Y. Sun, J. Li, Y. Du and N. Tang, *Phys. Rev. B*, 2017, **96**, 155448.
19 P. F. Liu, L. Zhou, S. Tretiak and L. M. Wu, *J. Mater. Chem. C*, 2017, **5**, 9181–9187.
20 Y. Ma, Y. Jing and T. Heine, *2D Mater.*, 2017, **4**, 025111.
21 B. Wang, S. Yuan, Y. Li, L. Shi and J. Wang, *Nanoscale*, 2017, **9**, 5577–5582.
22 L. Z. Zhang, Z. F. Wang, S. X. Du, H. J. Gao and F. Liu, *Phys. Rev. B: Condens. Matter Mater. Phys.*, 2014, **90**, 161402(R).
23 H. Zhang, Y. Li, J. Hou, A. Du and Z. Chen, *Nano Lett.*, 2016, **16**, 6124–6129.
24 Y. Jiao, F. Ma, J. Bell, A. Bilic and A. Du, *Angew. Chem., Int. Ed.*, 2016, **55**, 10292–10295.
25 S. Y. Xie, X. B. Li, W. Q. Tian, N. K. Chen, Y. Wang, S. Zhang and H. B. Sun, *Phys. Chem. Chem. Phys.*, 2015, **17**, 1093–1098.
26 J. Li, X. Fan, Y. Wei, J. Liu, J. Guo, X. Li, V. Wang, Y. Liang and G. Chen, *J. Mater. Chem. C*, 2016, **4**, 10866–10875.
27 G. Kresse and J. Furthmüller, *Phys. Rev. B: Condens. Matter Mater. Phys.*, 1996, **54**, 169–186.
28 J. P. Perdew, K. Burke and M. Ernzerhof, *Phys. Rev. Lett.*, 1996, **77**, 3865–3868.
29 G. Kresse and D. Joubert, *Phys. Rev. B: Condens. Matter Mater. Phys.*, 1999, **59**, 1758–1775.
30 J. Heyd, G. E. Scuseria and M. Ernzerhof, *J. Chem. Phys.*, 2003, **118**, 8207–8215.
31 A. Togo, F. Oba and I. Tanaka, *Phys. Rev. B: Condens. Matter Mater. Phys.*, 2008, **78**, 134106.
32 G. J. K. Martyna, M. L. Klein and M. Tuckerman, *J. Chem. Phys.*, 1992, **97**, 2635–2643.
33 D. Jose and A. Datta, *Acc. Chem. Res.*, 2014, **47**, 593–602.
34 T. K. Mandel, D. Jose, A. Nijamudheen and A. Datta, *J. Phys. Chem. C*, 2014, **118**, 12115–12120.
35 A. Nijamudheen, R. Bhattacharjee, S. Choudhury and A. Datta, *J. Phys. Chem. C*, 2015, **119**, 3802–3809.
36 C. Chowdhury, S. Jahiruddin and A. Datta, *J. Phys. Chem. Lett.*, 2016, **7**, 1288–1297.
37 C. Chowdhury and A. Datta, *J. Phys. Chem. Lett.*, 2017, **8**, 2909–2916.
38 H. Tang and S. Ismail-Beigi, *Phys. Rev. Lett.*, 2007, **99**, 115501.
39 J. D. Zhang, X. L. Cheng and D. H. Li, *J. Alloys Compd.*, 2011, **509**, 9577–9582.
40 H. Zhang, Y. Li, J. Hou, K. Tu and Z. Chen, *J. Am. Chem. Soc.*, 2016, **138**, 5644–5651.
41 M. Gao, Q. Z. Li, X. W. Yan and J. Wang, *Phys. Rev. B*, 2017, **95**, 024505.
42 C. Kamal and M. Ezawa, *Phys. Rev. B: Condens. Matter Mater. Phys.*, 2015, **91**, 085423.
43 H. Sahin, S. Cahangirov, M. Topsakal, E. Bekaroglu, E. Akturk, R. T. Senger and S. Ciraci, *Phys. Rev. B: Condens. Matter Mater. Phys.*, 2009, **80**, 155453.
44 H. Zhang, D. Wu, Q. Tang, L. Liu and Z. Zhou, *J. Mater. Chem. A*, 2013, **1**, 2231–2237.
45 H. Zhang, X. Zuo, H. Tang, G. Li and Z. Zhou, *Phys. Chem. Chem. Phys.*, 2015, **17**, 6280–6288.
46 H. Zhang, Y. Liao, G. Yang and X. Zhou, *ACS Omega*, 2018, **3**, 10517–10525.
47 H. Zhang, X. Zhang, G. Yang and X. Zhou, *J. Phys. Chem. C*, 2018, **122**, 5291–5302.
48 H. Zhang, Y. Li, Q. Tang, L. Liu and Z. Zhou, *Nanoscale*, 2012, **4**, 1078–1084; H. Zhang, X. Li, X. Meng, S. Zhou, G. Yang and X. Zhou, *J. Phys.: Condens. Matter*, 2019, DOI: 10.1088/1361-648X/aafea4.
49 D. Malko, C. Neiss, F. Vines and A. Goerling, *Phys. Rev. Lett.*, 2012, **108**, 086804.
50 A. Savin, R. Nesper, S. Wengert and T. F. Fässler, *Angew. Chem., Int. Ed. Engl.*, 1997, **36**, 1808–1832.
51 T. Teshome and A. Datta, *J. Phys. Chem. C*, 2018, **122**, 15047–15054.
52 T. Teshome and A. Datta, *ACS Appl. Mater. Interfaces*, 2017, **9**, 34213–34220.
53 C. Chowdhury, S. Karmakar and A. Datta, *ACS Energy Lett.*, 2016, **1**, 253–259.